Contents lists available at ScienceDirect

Applied Energy

journal homepage: www.elsevier.com

Thermo-hydraulic analysis and numerical simulation of a parabolic trough solar collector for direct steam generation

Ahmed Amine Hachicha[a,*], Ivette Rodríguez[b], Chaouki Ghenai[a]

[a] Sustainable and Renewable Energy Engineering Department, University of Sharjah, P.O.Box 27272, Sharjah, United Arab Emirates
[b] Heat Engines Department, Universitat Politècnica de Catalunya-BarcelonaTech, Spain

ARTICLE INFO

Keywords:
Direct Steam Generation
Parabolic trough
Tow phase flow model
Thermal gradient
Efficiency

ABSTRACT

Direct Steam Generation (DSG) is one of the most promising alternatives for parabolic trough solar plants to replace the synthetic oil and reduce the electricity cost. The focus of this work is to develop a comprehensive optical and thermo-hydraulic model for the performance prediction of DSG process under real operating conditions. Pressure drop and heat transfer characteristics are determined considering the effect of the non-uniform heat flux distribution due to the concentration of the sunlight. A numerical-geometrical method based on ray trace and finite volume method techniques is used to determine the solar flux distribution around the absorber tube with high accuracy. A heat transfer model based on energy balance is applied to predict the thermal performances of the different flow regimes in the DSG loop. The thermo-hydraulic behavior of the different DSG sections i.e. preheating, evaporation and superheating is investigated under different operating conditions. The validity of the model has been tested by being compared with experimental data from DISS test facility and other available models in the literature. The study also presents a comparative study of the effect of different parameters on the thermal gradient around the absorber tube. The analysis shows that the highest thermal gradient is occurring in the superheating section with a high risk of thermal bending and a potential damage risk. The model is also capable to evaluate the efficiency of a DSG loop for different conditions and help to take the appropriate control strategies to avoid flow instabilities in the DSG rows.

Nomenclature

Greek symbols

α	absorptance factor
γ	intercept factor
ϵ	emissivity
ε/D	relative roughness factor
θ	circumferential direction(°)
ρ	density (kg/m^3)
ϱ	reflectance
ζ	Focal distance alteration due to bending
μ	dynamic viscosity (Pa s)
ν	kinematic viscosity (m^2/s)
σ	Stefan-Boltzmann constant (5.67×10^{-8}W/m^{2}K^4)
σ_t	surface tension (N/m)
τ	transmittance
φ	incident angle (°)

Roman symbols

A	area(m^2)
B_o	Boiling number
C_p	specific heat (J/Kg K)
D	diameter (m)
e	thickness (m)
E	eccentricity (m)
f	friction coefficient
f_o	focal distance (m)
Fr	Froude Number (G^2/ρ^2gD)
g	gravity (m/s^2)
G	mass flux (kg/m^{2}s)
h	enthalpy (J/kg)
hc	convective heat transfer coefficient (W/m^{2}K)
I	irradiation per unit length (W/m^2)

* Corresponding author.
Email address: ahachicha@sharjah.ac.ae (A.A. Hachicha)

https://doi.org/10.1016/j.apenergy.2018.01.054
Received 25 October 2017; Received in revised form 16 January 2018; Accepted 22 January 2018
Available online xxx
0306-2619/

k	thermal conductivity (W/m K)
$\dot{m}$	mass flow rate (kg/s)
M	molecular mass of water (g/mol)
N	number of control volumes
Nu	Nusselt number (hcD/k)
P	pressure (N/m^2)
Pr	Prandtl number ($\mu c_p/k$)
$\dot{q}$	heat flux per unit of area (W/m^2)
r	radius (m)
R	two phase flow multiplier
Ra	Rayleigh number
Re	Reynolds number (UD/ν)
T	temperature (K)
u	velocity (m/s)
U_L	Overall heat transfer coefficient (W/m^{2}K)
W_e	Weber number ($G^2D/\rho\sigma_t$)
$\dot{x}$	quality
X	Martinelli parameter
z	axial coordinate (m)

Subscripts

1ph	one phase
2ph	two phase
a	absorber
abs	absorbed radiation
amb	ambient
cond	conduction
conv	convection
e	environment
eff	effective
g	glass
Gni	Gnielinski
HTF	heat transfer fluid
i	index of the control volume in the axial direction
in	input
j	index of the control volume in the azimuthal direction
max	maximum
NB	Nucleate Boiling
out	Output
rad	radiation
u	useful
w	wall

1. Introduction

In the last century, special attention has been given to renewable energy resources due to the increase of energy demand and climate threats. Solar energy is considered one of the most attractive and competitive alternatives to provide green, renewable and low-cost energy. In the specific case of solar thermal processes at high temperature, the parabolic trough solar collector is one of the most mature and prominent solar thermal technologies for electricity production and steam generation in industrial processes such as drying, sterilization process and water desalination [1–4].

Currently, the majority of commercial parabolic trough solar plants for electricity generation use synthetic oil as heat transfer fluid. However, Direct Steam Generation (DSG) is one of the most competitive technologies for the next generation of parabolic trough collectors (PTC) power plants. Unlike the synthetic oil-based technology, DSG technology uses directly concentrated solar flux to generate steam in the parabolic trough collectors. A significant cost reduction, by about 15%, can be achieved when using DSG due to the simplification of the plant layout by eliminating the intermediate heat exchanger between the solar field and the power block and the use of the synthetic oil as heat transfer fluid in the solar loop. As a result, the operation and maintenance costs of the solar plant can be considerably decreased [1]. According to a previous cost study, the levelized cost of electricity of the DSG process can be 11% lower than that of synthetic oil in a concentrated solar power (CSP) plant without thermal storage system [5]. In addition, the use of water/steam as heat transfer fluid enables the possibility of working at higher temperatures than with oils whereas at the same time eliminates the environmental risk of toxic oil leakage.

However, power plants based on DSG might lead to a more complex thermo-hydraulic process [6,7]. On the one hand, the thermal performance of the PTC plants is affected in the steam phase section due to the sudden decrease of the heat transfer coefficient. Different techniques to circumvent this issue have been proposed in the literature such as inserting foams [8], introducing helically finned tubes [9] or using curved absorber tubes [10,11]. On the other hand, the effect of two-phase flow on the stability and controllability of such solar plants is the major challenge in the commercialization of this technology. Recently, Guo et al. [12] proposed a dynamic model with the objective of improving the performance and robustness of the solar field. Other problems that might be encountered when operating when operating a DSG plant are the higher vapor pressure of water which forces the operation of this technology at higher pressures which can impose some additional costs for suitable hydraulic components. In addition, the lack of a suitable thermal energy storage is a potential barrier for commercial deployment of DSG solar plants although different alternatives [13–16] are currently being studied.

The resultant flow pattern inside the receiver is the consequence of the interaction between phases and instabilities occurring during the DSG process [17]. Different flow patterns can be observed during steam generation process such as: bubbly flow, plug flow, slug flow, stratified flow and annular flow. In practice, the stratified flow has the highest thermal stress risk due to the overheating in the dry section which may lead to the bending of the absorber tube [18,19]. On the other hand, the annular flow represents the most favorable flow pattern as it maintains the contact between water and the absorber pipe. Therefore, understanding the thermo-hydraulic behavior of the DSG process is required to ensure better controllability and minimize the temperature difference around the circumference of the absorber tube. In this context, the prediction of the thermal performance of parabolic trough solar collectors used for hot water and steam generation is an essential tool for the observation, operation, safety monitoring and certification of these solar collectors.

According to the state of the art of PTC technology, several models have studied the thermo-hydraulic characteristics of the one-phase flow synthetic oil as a heat transfer fluid [20–26]; however, DSG models are less presented in the literature.

An earlier DSG model was proposed by Odeh et al. [27] to evaluate thermal losses and performance of a DSG collector for different conditions. An efficiency equation and heat transfer coefficients were proposed to solve the two-phase flow under uniform heat flux using the correlation of Gunger and Winterton [28]. Later, Odeh et al. [29] carried out a hydrodynamic analysis using the flow pattern map proposed by Taitel [30]. In their analysis, a pressure drop model was proposed for both horizontal and inclined solar absorbers for once through DSG application. Eck and Steinmann [31] used the finite element method (FEM) ANSYS package to investigate the thermo-hydraulic behavior of the LS-3 absorber of the DISS facility considering a Gaussian distribution assumption for the solar flux on the outer circumference. Their numerical model was based on the correlation of Friedel [32] for the two-phase pressure drop calculation and the correlation of Gunger and Winterton [28] for heat transfer calculation. They proposed the insertion of

a control valve at the inlet of the evaporator collector loop to avoid flow instabilities.

Recently, several software tools have been proposed to solve the thermo-hydraulic behavior inside a DSG collector. Several commercial computational fluid dynamic CFD models were used to solve the superheated steam section [33,6] and for the whole DSG loop [19,34]. In these studies, the CFD model solves the thermo-hydraulic behavior inside the absorber pipes without considering the realistic non-uniform flux around the absorber tube for the three different sections (preheating, boiling and superheating). Other DSG models were based on numerical tools such as Modelica language [35,36], RELAP [37], ATHLET [38] and TRNSYS [39] for dealing with the dynamic simulation of DSG parabolic trough solar collectors. Elsafi [6] presented a complete flow pattern analysis along the DSG absorber tube and discussed the flow transitions in different sections of the DSG loop considering a constant heat flux distribution around the receiver. In his work, the flow pattern map proposed by Wotjan et al. [40] was used to predict the flow pattern in the DSG loops. Li et al. [41] proposed a coupled 2D-FVM and 3D-FEM models to study the thermo-elastic behavior of the absorber tube and provided a thermal bending analysis for different radiation angles. Recently, Hachicha [42] investigated the thermal performance of the one phase flow sections (water and steam) in a DSG process and extended his work to study the two-phase flow [43].

Despite the various numerical studies to predict the thermo-hydraulic behavior of the DSG process, the modeling of water-steam flow in parabolic trough collectors is still challenging [44]. According to the state of the art of DSG modeling, no previous work has been conducted to predict the thermo-hydraulic behavior and performance of the DSG process under the realistic non-uniform solar flux. The study of the temperature distribution around the DSG receiver is relevant not only to describe the interaction between the existing temperature gradients in the absorber tube and the two-phase flow which may induce a high level of thermal stress causing the bending of the absorber tube, but also to look for appropriate alternatives for reducing the large thermal gradients encountered specially in the steam phase.

It becomes obvious from the aforementioned literature that modeling the thermo-hydraulic process of DSG by applying the realistic non-uniform solar flux on the circumference of the absorber tube is essential to understand the mode of operation and thermal stress in the DSG loop.

In this paper, a comprehensive optical and thermo-hydraulic model is proposed to determine the temperature and pressure drop in the DSG process taking into consideration the effect of the non-uniform heat flux distribution due to the concentration of sunlight. The proposed methodology is an extension of a previous model developed for one phase flow PTC and is developed to predict the thermo-hydraulic behavior in the different sections of the DSG process. The methodology includes a numerical-geometrical model to simulate the realistic non-uniform solar flux distribution around the solar receiver while considering the influence of bending and conic eccentricity. The optical model is then coupled with a thermo-hydraulic model based on energy balances to determine the heat transfer characteristics and pressure drop within the DSG sections under different operating conditions. The present methodology is capable of predicting the behavior of a PTC for DSG and the variation of its performance under realistic working conditions. Moreover, it can be also used for the design and prediction of the thermo-hydraulic behavior of a DSG loop for a CSP plant.

2. Optical model

The optical modeling of the solar absorber in the DSG loop is essential to provide accurate solar flux distribution in the azimuthal direction. By neglecting the dependence of the optical parameters on temperature, the results of the optical model will be independent of temperature. Therefore, it can be implemented as a pre-processing task and coupled directly with the thermo-hydraulic model at the outer boundary condition of the absorber tube. A typical solar flux distribution per 1 kW/m^2 of incident radiation is presented in Fig. 1 for LS-3 PTC collector [1] at the peak optical efficiency condition. This distribution depends on several parameters such as geometric concentration, rim angle, incident angle and optical errors.

Most of the existing optical models simplify this distribution with a Gaussian [31] or rectangular [33] profile which has some error respect to realistic distribution. Other optical models [6,26,45] use a complex stochastic Monte Carlo Method which has a high computational cost.

The methodology adopted in this work to simulate the non-uniform distribution of the solar flux around the solar absorber is based on the extension of a previous optical model which uses the finite volume method (FVM) and ray tracing techniques [21]. This numerical-geometrical method allows tracking the finite size of the Sun and determining with high accuracy the distribution of the concentrated solar flux in the azimuthal direction. The entire domain of the parabolic trough solar collector is discretized in various grid systems while the solar optic cone is divided in symmetrical rays similar to the FVM (see Fig. 2). The optical properties are introduced in the calculation of the reflected rays that reach the absorber tube. The model starts by gener-

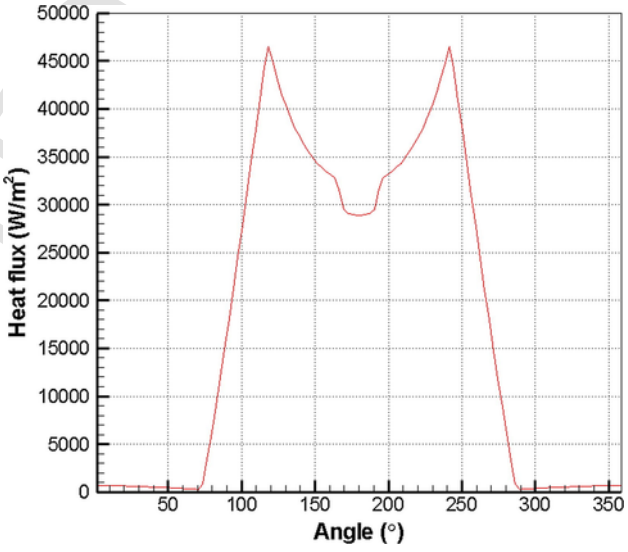

Fig. 1. Typical heat flux distribution along the outer surface of an LS-3 collector.

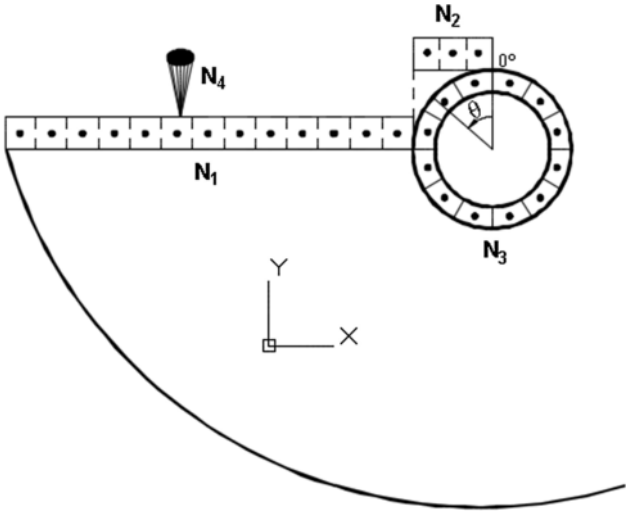

Fig. 2. Different grid systems used in the optical model.

ating rays at the parabola domain and discretizing the optic cone coming from the Sun.

The absorber tube is then discretized in different control volumes (CVs) in the azimuthal direction. Each CV intercepts the rays coming from the solar optic cone after specular reflection in the collector parabola. The integration of all rays intercepted by an absorber CV gives the total absorbed solar flux (for a more detailed explanation on the discretization used the reader is referred to [21]).

$$\dot{q}_{abs} = (\tau\alpha)_{eff}\rho\gamma\cos\varphi \sum I_{intercepted} \quad (1)$$

The model includes the optical errors in what is called intercept factor γ and also the effect of the incident angle [6]. The previous optical model has been improved to take into consideration the effects of other optical errors that can change not only the magnitude of the absorbed solar flux but also the profile, namely eccentricity and thermal bending.

Eccentricity is the slight change of the parabola aperture due to the weight of the mirrors and brackets. The analytical coordinate of the parabola due to the conic eccentricity E is expressed by the following equation [6]:

$$y = \frac{E}{1-E^2}\left[2f_o - \left(4f_o^2 + x^2(1-E^{-2})\right)^{1/2}\right] \quad (2)$$

The model includes the optical errors caused by bending which may occur due to the high thermal gradients applied on the circumference of the tube. This kind of error leads to a slight displacement of the absorber tube with respect to the focal line. The maximum bending occurs at the central section of the absorber tube and can be modeled with the following relation

$$\Delta_{f_o,\max} = \zeta(r_g - r_a) \quad (3)$$

To illustrate these effects, the present methodology has been used to determine the solar flux distribution around the LS-3 absorber. Fig. 3 shows this distribution for different conic eccentricity and displacement of the absorber tube as a result of the thermal bending. It is shown that eccentricity leads to an increase and shift of the heat flux peak towards the mid plane of the absorber tube, while the bending of the absorber tube results in a decrease and broadening of the solar flux distribution due to the displacement of the tube out of the focus of the parabola.

3. Mathematical model

The present thermo-hydraulic model is based on an energy balance about the heat collector element (HCE) to predict the performance of a DSG collector using water-steam as a heat transfer fluid (HTF). The general modeling approach is based on the finite volume method, where an energy balance is performed on each control volume of the HCE. The numerical model includes the optical and thermal losses around the HCE. For a detailed description of the discretization used along the azimuthal direction of the HCE, the reader is referred to Hachicha et al. [21].

3.1. Thermal model

A one-dimensional step-by-step method is used to determine the heat gain by the HTF in the axial direction. The fluid domain is divided into N_x control volumes in the axial direction, while the HCE is discretized in both axial and azimuthal directions (N_x, N_ϕ) considering the non-uniform distribution of the solar flux (see previous section). Considering that the change of kinetic and potential energies is negligible, the steady-state energy balance in one control volume is expressed as

$$\sum_j \dot{q}_{u,ij}A_j + \dot{m}(h_{i,in} - h_{i,out}) = 0 \quad (4)$$

where $\dot{q}_{u,ij}$ is the useful thermal energy per unit area and h is the fluid enthalpy evaluated at the control volume face. The heat gain is calculated taking the difference between the absorbed solar radiation and the heat losses for each segment.

$$\dot{q}_{u,ij} = \dot{q}_{abs,ij} - \dot{q}_{loss,ij} = \dot{q}_{cond,a} = \dot{q}_{conv,HTF-a} \quad (5)$$

The absorbed solar radiation is determined using the optical model, considering the optical characteristics as well as the optical errors encountered in the PTC technology.

To estimate the thermal losses from the PTC receiver tube, a steady-state energy balance model (see Fig. 4) is adopted and different heat fluxes are calculated. The energy balance applied on the heat collector element can be expressed as

$$\begin{aligned}\dot{Q}_{loss} &= \dot{Q}_{conv,a-g} + \dot{Q}_{rad,a-g} \\ &= \dot{Q}_{cond,g} \\ &= \dot{Q}_{conv,g-e} + \dot{Q}_{rad,g-e}\end{aligned} \quad (6)$$

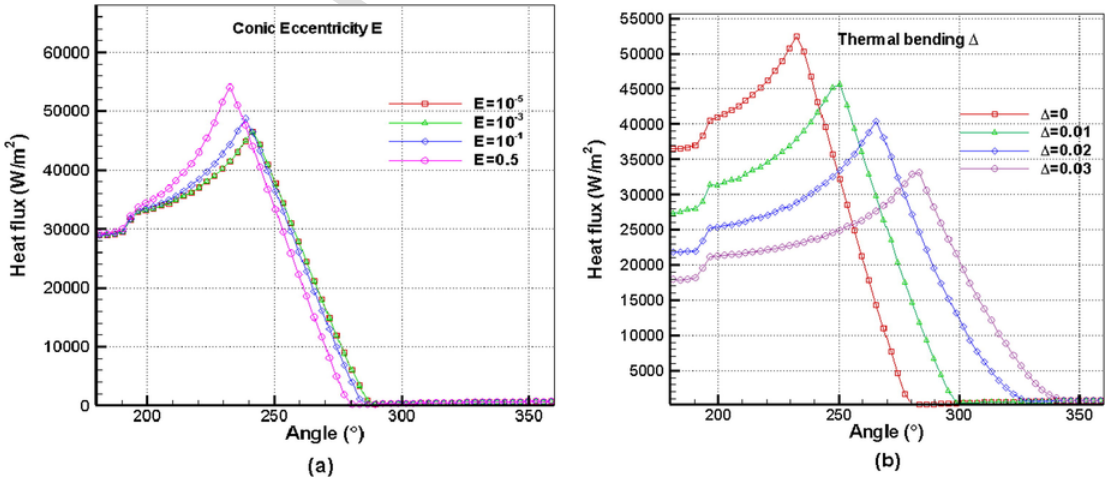

Fig. 3. Effect of (a) eccentricity; (b) bending on the solar flux distribution around a typical LS-3 PTC.

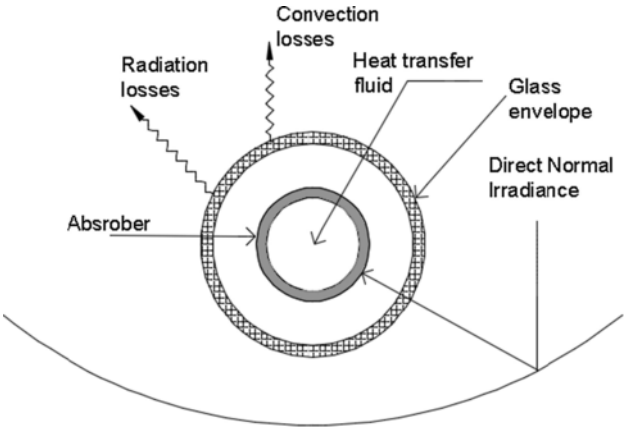

Fig. 4. Energy balance model applied on a cross section of the HCE.

Heat losses from the absorber tube are mainly transferred by radiation $\dot{Q}_{rad,a-g}$ between the outer absorber tube and the inner glass tube. The convection between the absorber tube and glass tube $\dot{Q}_{conv,a-g}$ is neglected as there is vacuum in this annular zone. $\dot{Q}_{cond,g}$ is the heat conduction through the glass envelope, which is exchanged again by convection to the ambient $\dot{Q}_{conv,g-e}$ and radiation between the glass envelope and the sky $\dot{Q}_{rad,g-e}$.

Radiation heat transfer between the absorber tube and the glass cover $\dot{Q}_{rad,a-g}$ is determined by applying the net radiation method to the cross section of the HCE, considering the surfaces of the absorber and glass tubes as being grey and diffuse emitters and reflectors. The Hottel's crossed-string method is used to calculate the view factors and the net radiation flux is determined by considering the radiation exchange in each control volume [21].

Heat conduction through the absorber tube/glass cover is determined using Fourier's law in both axial and azimuthal directions.

$$\dot{q}_{cond,axial} = -\frac{\partial(kT)}{\partial z}A_z$$

and

$$\dot{q}_{cond,azimuthal} = -\frac{\partial(kT)}{r\partial\theta}e$$

where A_z, e are the cross-section area and thickness of the absorber tube/glass cover control volume, respectively.

Outside the solar absorber, convection heat transfer with the ambient can happen in the presence or absence of the wind. Under forced convection, i.e. in presence of wind, the correlation of Churchill and Bernstein [46] is considered for RePr > 0.2.

$$Nu = 0.3 + \frac{0.62Re^{0.5}\mathrm{Pr}^{1/3}}{[1+(0.4/\mathrm{Pr})^{2/3}]^{1/4}}\left[1+\left(\frac{Re}{282{,}000}\right)^{5/8}\right]^{4/5} \quad (7)$$

Otherwise, natural convection is held in the absence of the wind with the Churchill and Chu correlation [46] for the Nusselt number calculation

$$Nu = \left[0.6 + \frac{0.387Ra^{1/6}}{[1+(0.599/\mathrm{Pr})^{9/16}]^{8/27}}\right]^2 \quad (8)$$

For the radiation heat transfer with the ambient, the absorber tube is considered as a small grey object in a large black body, the sky, and is evaluated with the following expression

$$\dot{q}_{rad,e} = \sigma\epsilon(T_a^4 - T_{sky}^4) \quad (9)$$

Alternatively, thermal losses can also be estimated by defining an overall heat loss coefficient which depends on the temperature difference between the absorber tube and ambient.

$$\dot{Q}_{loss} = AU_L(T_a - T_{amb}) \quad (10)$$

If the data for the specific absorber tube is known, a different approach can be used by approximating the overall heat loss coefficient to the experimental data.

$$U_L = a_1 + a_2(T_a - T_{amb}) + a_3(T_a - T_{amb})^2 \quad (11)$$

Note that as the above equation is the result of a curve-fitting from experimental measurements, a_1, a_2 and a_3 correlation coefficients have to be defined. In Table 1, the values for the LS-3 collector obtained in [47] are given.

The useful thermal energy is transferred to the heat transfer fluid through forced convection with the inner surface of the absorber tube. Under steady-state conditions, convection inside the absorber tube is governed by the Newton's law.

$$\dot{q}_{conv,HTF-a} = hc(T_{a,ij} - T_{HTF,i}) \quad (12)$$

The convection heat transfer coefficient ($h_c = \mathrm{Nu}\ k/D$) is evaluated as a function of the Nusselt number depending on the flow phase in the DSG loop as explained in the following sub-sections.

3.2. Single-phase flow modeling

The thermo-hydraulic modeling of water-steam inside the absorber tube is based on the prediction of heat transfer coefficient and pressure gradient.

For a single-phase flow in the preheating or superheating sections, the Nusselt number and the pressure gradient can be estimated based on experimental correlations. In practice, the flow inside the DSG loop is always turbulent and the Nusselt number can be estimated using the Gnielinski correlation [48] as showing below

$$Nu = \frac{(f_{Gni}/8)(Re-1000)\,\mathrm{Pr}}{1+12.7\sqrt{(f/8)}(\mathrm{Pr}^{2/3}-1)}\left(\frac{\mathrm{Pr}}{\mathrm{Pr}_w}\right)^{0.11} \quad (13)$$

with $f_{Gni} = (1.82\log(Re) - 1.64)^{-2}$.

In this correlation, fluid properties are evaluated at the HTF average temperature except Pr_w which depends on the temperature of the absorber inner surface. Note that this correlation is only valid for $0 < Pr < 2000$ and $2300 < Re < 5\cdot10^6$. However, in practice, most of the studied flows are within these ranges. The heat transfer coefficient under the single-phase flow condition can be obtained from the Nusselt number as $hc_{1ph} = \frac{Nu\ k}{D}$.

The pressure drop for turbulent single-phase water or steam is calculated using the Blasius equation

Table 1
Curve-fitting coefficients for U_L for the LS-3 collector [47].

T_a	a_1	a_2	a_3
<200	0.687257	0.001941	0.000026
≤300	1.433242	−0.00566	0.000046
>300	2.895474	−0.01640	0.000065

$$\Delta p_{1ph} = \frac{f_{1ph} dz}{D_{ai}} \left(\frac{1}{2} \rho_{1ph} u_{1ph}^2 \right) \tag{14}$$

where f_{1ph} is the friction factor for turbulent flow, which is determined by using Moody's friction factor correlation [49] considering the relative surface roughness ($\frac{\varepsilon}{D_{ai}}$):

$$f_{1ph} = 0.0055 \left[1 + \left(20{,}000 \frac{\varepsilon}{D_{ai}} + \frac{10^6}{Re_{1ph}} \right)^{\frac{1}{3}} \right] \tag{15}$$

3.3. Two-phase flow modeling

When the heat transfer fluid reaches the two-phase flow regime, the modeling of the heat transfer and pressure drop becomes much more complex and depends on the flow pattern map. In the evaporator section, where the two-phase flow occurs, different flow patterns and thus different phase distributions can be observed.

3.3.1. Heat transfer coefficient

In this work, the heat transfer coefficient is evaluated based on the map developed by Odeh [27]. In the DSG loop, it is recommended to avoid stratified flow which leads to higher temperature gradients and may provoke the failure of the heat collector element. Therefore, it is important to know the flow patterns and the effect of the absorbed solar radiation and the steam quality.

In the aforementioned flow pattern map, the flow transition is determined using the dimensionless Froud number. This number is defined as the ratio of the flow inertia to the gravity force.

$$Fr = \frac{G^2}{\rho_{1ph}^2 g D_i} \tag{16}$$

If Fr < 0.04, the flow is stratified and the heat transfer coefficient can be determined using Shah equation [28].

$$\frac{h_{2ph}}{h_l} = 3.9 Fr^{0.24} \left(\frac{\dot{x}}{1 - \dot{x}} \right)^{0.64} \left(\frac{\rho_l}{\rho_g} \right)^{0.4} \tag{17}$$

where h_{2ph} is the two-phase flow heat transfer coefficient and x is the steam quality. In the above expression, l and g sub-indexes stand for the liquid and steam phases, respectively. The liquid heat transfer coefficient h_l is determined using the single-phase flow correlation considering the liquid fraction inside the absorber tube, i.e. the Reynolds number in the Gnielinski correlation (Eq. (13)) is substituted with $Re_l = \frac{G(1-\dot{x})}{\mu_l}$.

If Fr > 0.04, annular flow occurs inside the absorber tube. In this case, the heat transfer coefficient is evaluated using Chen correlation [28] which is divided into two components: a nucleate boiling contribution and a single-phase convection contribution for saturated water.

$$h_{2ph} = S h_{NB} + E h_l \tag{18}$$

The suppression factor S and the enhancement factor E are given by Gunger and Winterton [28]

$$S = (1 + 1.15 \cdot 10^{-6} E^2 Re_l^{1.17})^{-1} \tag{19}$$

$$E = 1 + 24{,}000 B_o^{1.16} + 1.37 X^{-0.86} \tag{20}$$

Here, boiling number is $B_0 = \dot{q}_{abs} / \dot{m} (h_g - h_l)$ whereas the Martinelli parameter X is given as

$$X = \left(\frac{1 - \dot{x}}{\dot{x}} \right)^{0.9} \left(\frac{\rho_g}{\rho_l} \right)^{0.5} \left(\frac{\mu_l}{\mu_g} \right)^{0.1} \tag{21}$$

In this correlation, the liquid heat transfer coefficient is given based on the Dittus-Boelter equation considering the fraction of liquid filling the absorber tube.

$$h_l = 0.023 \left(\frac{k_l}{D_i} \right) \left(\frac{G(1 - \dot{x}) D_i}{\mu_l} \right)^{0.8} (\mathrm{Pr})_l^{0.4} \tag{22}$$

In the wetted and heated region of the annular flow, the nucleate boiling heat transfer coefficient hc_{NB} can be estimated as

$$h_{NB} = 55 p_r^{0.12} (-\log_{10} p_r)^{-0.55} M^{-0.5} q_{abs}^{0.67} \tag{23}$$

where the reduced water pressure $p_r = p/p_c$ is the ratio between the working pressure and the critical pressure of water (221 bar).

3.3.2. Pressure drop

The pressure drop is calculated using the Friedel correlation which has been proven to be the most accurate model during the European DISS project [31]. In this correlation, a two-phase flow multiplier R is defined to correct the single-phase flow pressure drop Δp_{1ph} obtained by Blasius equation.

$$\Delta p_{2ph} = R \Delta p_{1ph} \tag{24}$$

$$R = A + 3.43 x^{0.685} (1 - \dot{x})^{0.24} \left(\frac{\rho_l}{\rho_g} \right)^{0.8} \left(\frac{\mu_g}{\mu_l} \right)^{0.22} \left(1 - \frac{\mu_g}{\mu_l} \right)^{0.89} Fr_l^{-0.047} We_l^{-0.0334}$$

$$A = (1 - \dot{x})^2 + \dot{x}^2 \left(\frac{\rho_l \xi_g}{\rho_g \xi_l} \right) \tag{26}$$

where *We* ($We_l = \frac{G^2 D_i}{\rho_l \sigma}$), ξ_g and ξ_l are the Weber dimensionless number, vapor friction coefficient and liquid friction coefficient, respectively.

The vapor friction coefficient is determined for turbulent steam/water ("g/l") flow ($Re_{g/l} > 1055$) as follows:

$$\xi_{g/l} = \left[0.86859 \log \left(\frac{Re_{g/l}}{1.964 \log(Re_{g/l}) - 3.8215} \right) \right]^{-2} \tag{27}$$

If the steam/water flow is laminar ($Re_{g/l} < 1055$).

$$\xi_{g/l} = \frac{64}{Re_{g/l}} \tag{28}$$

3.4. Numerical procedure

The numerical procedure starts by discretizing the absorber tube into several control volumes in both longitudinal and azimuthal directions. The general algorithm is divided in two main parts: optical modeling to determine the solar flux distribution around the absorber tube and thermo-hydraulic model to predict the heat transfer coefficient and pressure drop of the water-steam flow inside the DSG loop.

In the optical model, the solar flux distribution is determined using the numerical-geometrical model taking into account the optical errors and incident angle (see Section 2). The obtained solar flux distribution is coupled with the thermo-hydraulic model as a boundary condition for the absorber surface by assuming the solar absorption as a surface phenomenon.

In the thermo-hydraulic model, the properties of the heat transfer fluid (water/steam) are determined using the International Association for Properties of Water IAPWS-IF 1997 standard [50]. The inlet quality is calculated based on the inlet conditions of the DSG loop. The different heat fluxes are then calculated for each control volume after initializing the temperature maps and setting the material properties.

Using the meteorological data and the results of the optical model, the outlet enthalpy at each fluid CV can be determined from Eq. (3). Depending on the nature of the phase flow, i.e. single-phase flow or two-phase flow, the heat transfer coefficient and the pressure drop are determined using the equations outlined before. The pressure drop calculations yield to a new pressure at the outlet of the fluid CV, while the calculation of the heat transfer coefficient allows to estimate the temperature of the adjacent absorber CV. Once the outlet pressure and enthalpy are known for each fluid CV, the outlet fluid temperature is evaluated using the backward equations from IAPWS-IF97. The outlet properties of one fluid CV are considered as the inlet properties for the next control volume.

This procedure is repeated along the heat collector element and the global convergence is achieved once the fluid temperature becomes fully stable for each control volume in the HTF domain, i.e., when the temperature difference between the current iteration and the previous one is less than $\varepsilon = 10^{-6}$. The general algorithm of the present model is presented in Fig. 5.

4. Model validation

In this section, first a brief description of the test loop is given following with a mesh sensitive analysis to optimize the number of control volumes. The present methodology is then validated with available experimental data in once-through DSG process by comparing the results with those obtained in the DISS test facility [6,19] at Plataforma Solar de Almeria (PSA).

4.1. System description

In direct steam generation trough collectors, the absorber tube is divided into three sections: single-phase water, two-phase flow and single-phase superheated steam [51]. In practice, there are three possible operation modes in a DSG loop: the once-through mode, the recirculation mode and the injection mode. Each of these configurations has some advantages and disadvantages, however, the once-through mode is considered the cheapest and simplest operation mode.

The validation is carried out in two steps: single-phase flow and two-phase flow. Experimental data are taken from the final results provided by the DISS test facility [6,19] at Plataforma Solar de Almeria (PSA). This facility consists of a row of 11 LS-3 type collectors (see Fig. 6). In this DSG loop, the first collector is used to preheat water to the saturation temperature, while the boiling section occurs between collector 2 and 10 and only the last two collectors are reserved for the superheating section. In this facility, various thermocouples are mounted in different sections along the absorber tube, where the azimuthal temperature is instrumented using 8 Type K thermocouple class I with an accuracy of 1.5 °C according to the standard IEC 60584.2. As per the pressure data, Rosemount 3051 pressure transmitters are used to measure the pressure drop which have an accuracy of 1.1%. The main specifications of the LS-3 collector and interconnections are given in Table 2.

4.2. Mesh sensitivity study

A mesh sensitive analysis is conducted to optimize the number of control volumes to be used in the DSG collector model. To do this, the mesh refinement level is set by fixing all the parameters and changing the number of control volumes in both axial and azimuthal directions.

The study case selected for the mesh test analysis is based on one of the experiments performed in the DISS test facility (DNI = 822 W/m^2, T_{in} = 205 °C, P_{in} = 3 bar, $\dot{m}$ = 0.47 kg/s). Thermal losses are estimated from the heat loss function of DISS-LS3 collectors [19] for the different DSG sections.

The grid system adopted in the optical model is similar to the one used in the previous work [21] for N1, N2 and N4. Only a grid independence study in N3 (or N_θ) was carried out to check the influence of the azimuthal direction on the optical model and the solar flux distribution. Fig. 7 shows the variation of the maximum heat flux at the outer wall of the absorber tube for different azimuthal coordinates.

The final number of nodes in the azimuthal direction has to be a compromise between accuracy and efficiency of the model. In this case, the number of control volumes in the azimuthal direction selected is $N_\theta = 120$ as it gives a relative error less than 2% with respect to the experimental data within a reasonable computational time.

A grid independence mesh study is also conducted on the longitudinal direction where the outlet conditions (temperature and pressure) are compared with the experimental results for the same studied case (see Fig. 8). The analysis showed a good convergence of the outlet variables with the axial direction after a mesh refinement of $N_x = 200$ with a relative error lower than 4%.

According to the independence mesh analysis in both longitudinal and azimuthal directions, the final mesh adopted in this work is $N_x = 200$ and $N_\theta = 120$.

4.3. Model validation results

A single-phase validation has been conducted and numerical results have been compared with the experimental data for superheated steam. Thermal losses are estimated based on the thermal-loss equation for the DISS-LS3 collector. The data are set for a typical LS-3 parabolic collector with a length of 4.06 m placed in the superheating section. All the optical and thermal parameters can be found in [6].

For validation purposes, data with different ranges of pressure (3MPa, 6 MPa and 10 MPa) and flow rates covering the working operation conditions are selected. The operation conditions and model inputs of the studied cases are presented in Table 3 together with experimental/numerical results.

As can be seen from Table 3, the numerical results are in good agreement with the experimental data. In all the cases, the root mean square (RMS) deviation is less than 0.05% for both the temperature and the pressure of the HTF at the outlet section.

The temperature distribution around the absorber tube is also here studied to understand the thermal gradient and thermal stress around the absorber tube. In Fig. 9, the temperature distribution in the azimuthal direction is compared for two cases with experimental results from Serrano-Aguilera et al. [6] at a cross section near the outlet edge of the absorber tube. The computed temperature distribution follows the same trend of the experimental measurements. Notice that there is a small scattering in the experimental data as the curves are not perfectly symmetric as in the numerical model.

Moreover, the small deviation from experimental results might also be attributed essentially to the thermal losses model equation adopted (Eqs. (10) and (11)) which includes all thermal losses in one equation without considering the loss variation in the azimuthal direction. It is

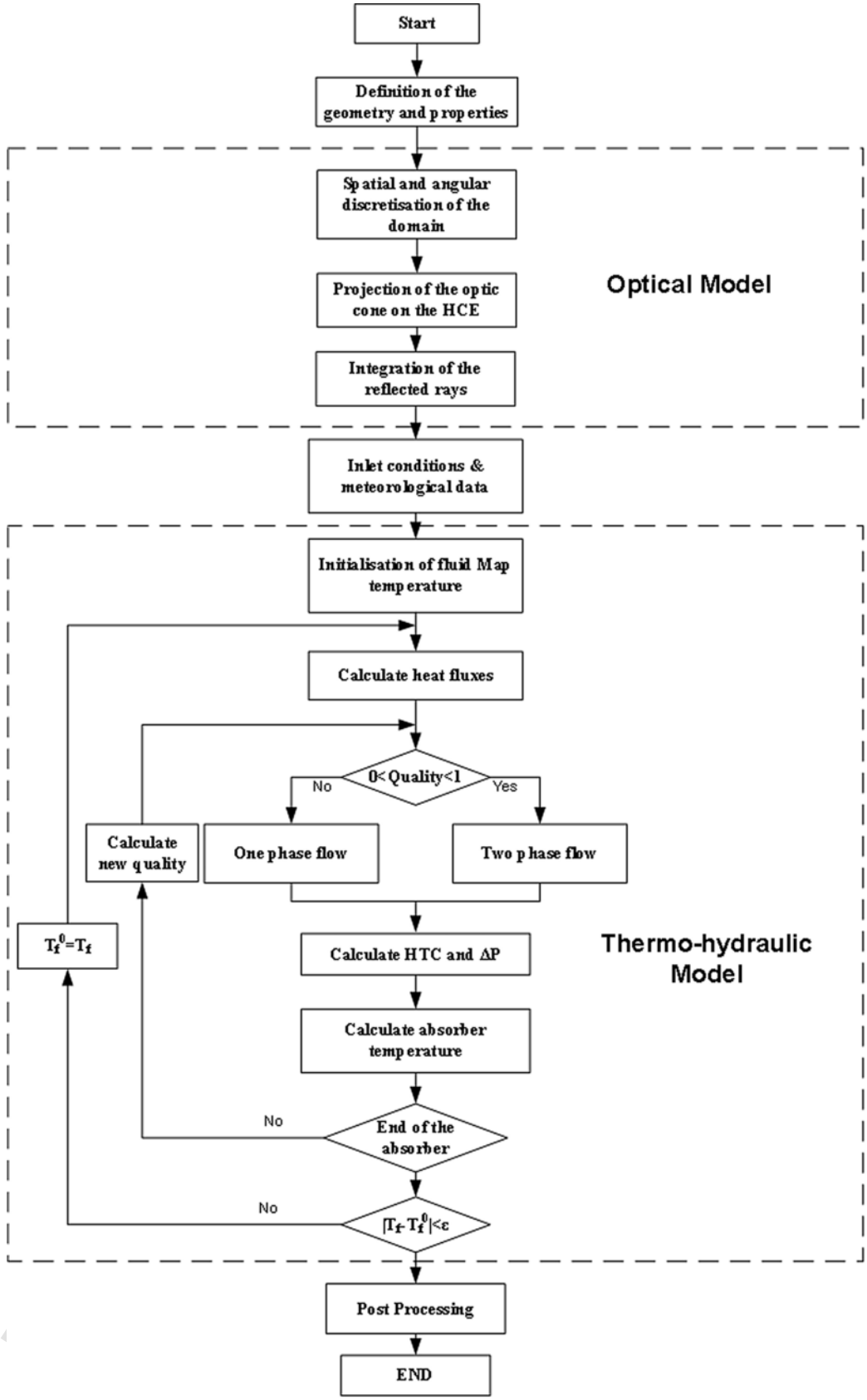

Fig. 5. Flow diagram of the general algorithm.

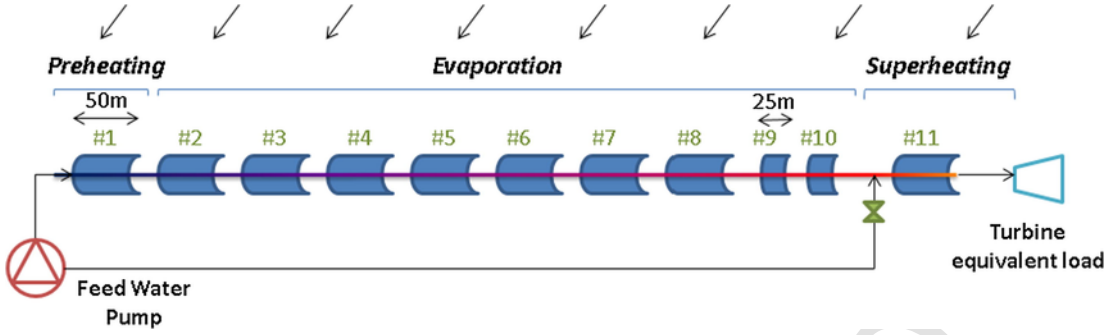

Fig. 6. The once-through mode in the DISS test facility [19].

Table 2
Main parameters of the LS-3 collector and interconnection pipes [19].

Aperture width (m)	5.76
Outer/inner diameter of absorber tube (m)	0.07/0.05
Overall length of a single collector (m)	50/25
Inner surface roughness of the steel absorber (m)	4E-05
Connection pipe between collector 1–8(m)	11
Connection pipe between collector 8–11 (m)	17
Number of 90° elbows between adjacent collectors	8
Peak optical efficiency (%)	77

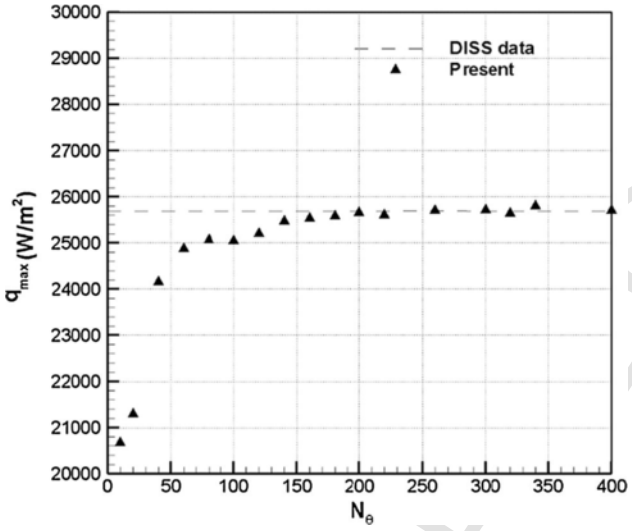

Fig. 7. Mesh test in the azimuthal direction. Comparison of the maximum solar flux at the outer wall of the absorber tube with experimental data from DISS facility [19].

also observed that thermal distribution around the absorber tube has a similar profile as the solar flux with the maximum temperature occurring in the lower part of the steel absorber tube.

The thermo-hydraulic model is also validated by carrying out the simulation for the entire DISS collector loop [19] with a total length of 510 m. In this simulation, the heat transfer coefficient and pressure

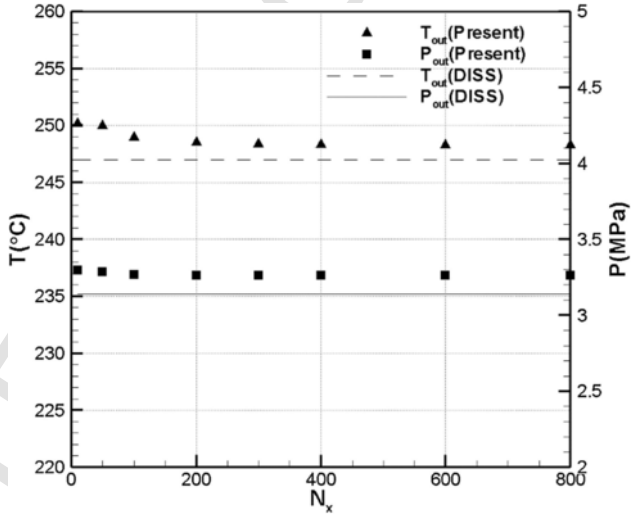

Fig. 8. Mesh test in the axial direction.

drop have been calculated along the absorber tube by checking the steam quality at each control volume. The inlet conditions and input parameters are selected from the DISS solar field test facility [19] as prescribed in Table 4.

The simulation includes three sections: preheating, evaporation and superheating, although the evaporation section fills almost 80% of the total length. The temperature and pressure fields have been calculated and compared with the experimental measurements. Fig. 10 shows the comparison of the temperature and pressure distribution along the DSG loop for two nominal operating pressures (3 and 6 MPa). Note that results for the lower pressure level (3 MPa) can be read in the left axis whereas the results for the higher-pressure level (6MPa) are presented on the right axis of both graphs.

It can be seen from Fig. 10a that the temperature experiences a steep increase in the first part of the DSG loop up until phase-change occurs. Then, in the middle section of the loop, the temperature remains almost constant to increase again in the super-heater section. In addition, the pressure drop increases from the preheating to the super-

Table 3
Operation conditions and experimental/numerical results for different cases.

Case	Experimental data							Numerical results	
	T_{in} (°C)	P_{in} (MPa)	$\dot{m}$	DNI	T_{amb}	T_{out} (°C)	ΔP (MPa)	T_{out} (°C)	ΔP (MPa)
Case1	254.65	3.223	0.5	790	307.9	261.95	0.0029	262.15	0.0028
Case2	259.65	3.237	0.52	771	309.6	266.75	0.0031	266.93	0.0031
Case3	286.85	6.188	0.64	921	303.3	291.85	0.0024	291.82	0.0023
Case4	278.45	6.125	0.53	804	307.2	283.35	0.0017	283.19	0.0015
Case5	343.35	10.085	0.58	853	307.0	261.95	0.0029	262.15	0.0028

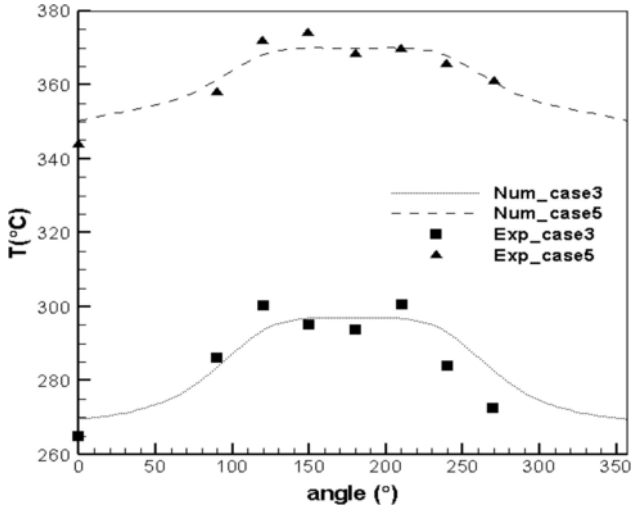

Fig. 9. Numerical results (Num) of the temperature distribution around the absorber tube compared with the DISS experiment (Exp) for two pressure ranges [6].

Table 4
Operation conditions for cases evaluated.

Case	T_{in} (°C)	P_{in} (MPa) (W/m^2)	ṁ	DNI	Max heat flux
Case1	205	3.42	0.47	822	25,686
Case2	239	6.25	0.55	971	30,316

heating section (see Fig. 10b), the largest pressure losses occur in the superheating section as the density of the fluid decreases.

In most of the cases the numerical results are within the experimental uncertainties range. However, some discrepancies are detected in the pressure drop at low pressure essentially due to the effect of flashing which is not considered in this model. Overall, the root mean square error for the outlet temperature and pressure is around 0.6% and 2.2%, respectively.

5. Model results

The present methodology can be used in different forms: (i) for designing a DSG for a CSP plant by selecting/testing the best combination of elements in the different parts of the loop; (ii) for evaluating the performance of a single PTC in either of the phases of the loop, i.e. for the single-phase pre-heating phase, for the two-phase evaporating section or for the single-phase superheating section of the loop; or (iii) for analyzing the performance of an existing DSG loop under different working conditions. In this section, the last two are considered for illustrating the capabilities of the present methodology.

In order to analyze how the working conditions affect the performance of the solar loop, a parametric study is conducted by changing different parameters such as pressure, temperature, direct normal irradiance, incident angle and rim angle. Case 1 (DNI = 822 W/m^2, T_{in} = 205 °C, P_{in} = 3.42 MPa, ṁ = 0.47 kg/s) from the DISS collector loop is considered as a baseline case for this analysis.

5.1. Effect of the pressure level on the loop

The effect of the pressure level on the loop has been considered by increasing the pressure at the inlet of the loop. In this case, pressure levels of 6 and 10 MPa have been selected.

Fig. 11 depicts the variation of the temperature difference between the highest and lowest temperature in the absorber cross section along the collector loop for the different operating pressures. The different DSG sections i.e. preheating, evaporation and superheating are clearly distinguished. The highest thermal gradient occurs in the superheating section where the heat transfer coefficient of the superheated steam is low to provide enough cooling for the absorber tube. It is apparent that the evaporation section presents the lowest thermal gradient because of the occurrence of annular flow characterized by a rapid increase of the heat transfer coefficient. The numerical results are consistent with the results of [31,51] with the same trend at different DSG sections. From Fig. 11, it can be seen that increasing the pressure is favorable for the increase of the occupation preheating section while decreasing the occupation of the evaporation section and thereby the annular flow [7].

The temperature difference between the absorber tube and fluid (water/steam) temperature is of special interest in designing the heat collector element and selecting the selective coating material to withstand such temperatures. Moreover, this temperature difference is also important when it comes to analyze the thermal stresses at which the absorber tube is submitted and thus the possibility of a larger bending of the heat collector element. Fig. 12 shows the comparison of the temperature difference between the absorber tube and the heat transfer fluid along the DISS loop for the different operating pressures (3 MPa, 6 MPa, 10 MPa). In this figure, it can readily be distinguished the sec-

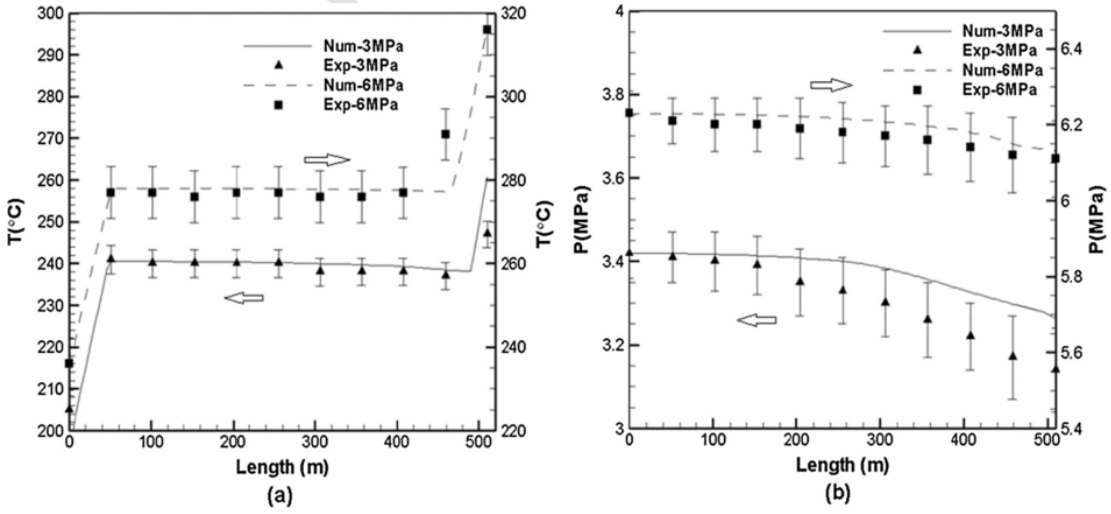

Fig. 10. Experimental (Exp) and computed results (Num) of temperature and pressure along the DSG loop for two operating pressure (3 MPa, 6 MPa). (a) Temperature (b) pressure.

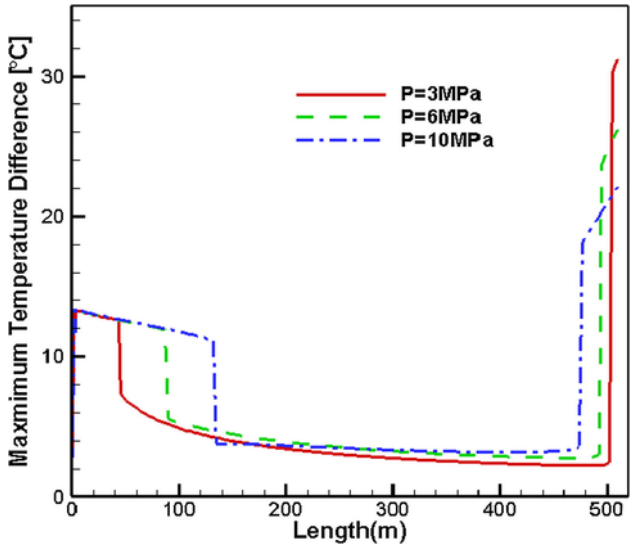

Fig. 11. Maximum temperature difference around the absorber tube for different operating pressures.

tions where phase-change occurs, which is similar to Fig. 11 (for the maximum temperature difference). The highest temperature difference between the absorber tube and water/steam occurs after the dry-out point in the superheating section. Notice also that the profile for the azimuthal distribution follows the solar radiation distribution, with maximum peaks close to azimuthal angle (120° and 240°).

The resultant distribution is in line with the results found by [31,41]. However, some discrepancies can be seen due to the operation modes and the solar distribution profile adopted. It is worth to note that in this work only the once-through operation mode was simulated and the realistic non-uniform solar distribution was calculated without simplification.

5.2. Effect of the inlet temperature

The effect of the inlet temperature along the DSG loop is also carried out by changing the temperature at the inlet of the DSG loop. Apart from the baseline case, two different temperature levels of $T_{in} = 220\,°C$ and $T_{in} = 240\,°C$ are also considered.

Fig. 13 shows the impact of the variation of the inlet temperature on the maximum temperature difference around the absorber tube. As expected, the increase of the temperature leads to the reduction of the preheating section and the increase of the annular flow in the evaporation section. However, the absorber tube exhibits a higher thermal gradient for a longer part of the loop at the superheating section when the inlet temperature is increased.

The graphical distribution of circumferential temperature difference between the absorber tube and the HTF is represented in Fig. 14. It is clearly observed that local overheating is likely to occur in the superheating section for higher inlet temperature which indicates higher thermal stress and risk of thermal bending.

5.3. Effect of the direct normal irradiance

Usually, solar field loops are designed for a determined direct normal irradiance. However, the performance of the loop can be seriously affected by the variation in the levels of irradiation the PTC receives. This is especially important in DSG loops where the level of irradiation affects the zones where pre-heating, evaporation and superheating is taking place. The variation of the thermal gradient around the absorber tube for different direct normal irradiances of 500 and 1000 W/m^2 is then investigated as shown Fig. 15. Compared to the baseline case, the increase of the DNI will slightly reduce the preheating section. However, as a consequence of higher heat gains in the HCE the evaporation section is considerably narrowed. At higher DNI, this reduction might be favorable to reduce the risk of the thermal stratification that might appear, whereas a larger evaporation section is observed at low DNI, which might result in the undesirable presence of stratified flow. The disadvantage of working at higher DNI is the higher thermal gradient observed in the superheating section which can peak up to 50 °C for an irradiance of 1000 W/m^2 with the consequently increased risk of thermal stress and bending of the HCE.

5.4. Effect of incidence angle

Fig. 16 shows the impact of the variation of the incident angle on the temperature difference of the absorber tube. In this simulation, the length of the DSG loop was increased to be able to detect the effect on the superheating section. It is clear that the effect of increasing the incident angle is quite similar to decreasing the DNI as they are correlated with the cosine effect. Therefore, it is recommended to work at higher irradiance and normal incident angle to avoid thermal stratification but attention should be paid to the high gradient in the superheating section.

5.5. Efficiency of the DSG process

In order to understand the influence of the two-phase flow conditions on the overall efficiency, the performance of the DSG loop has been evaluated in each section for the baseline case. The efficiency is determined based on the extent of each section. Fig. 17 shows the variation of efficiency with the direct normal irradiance along the collector

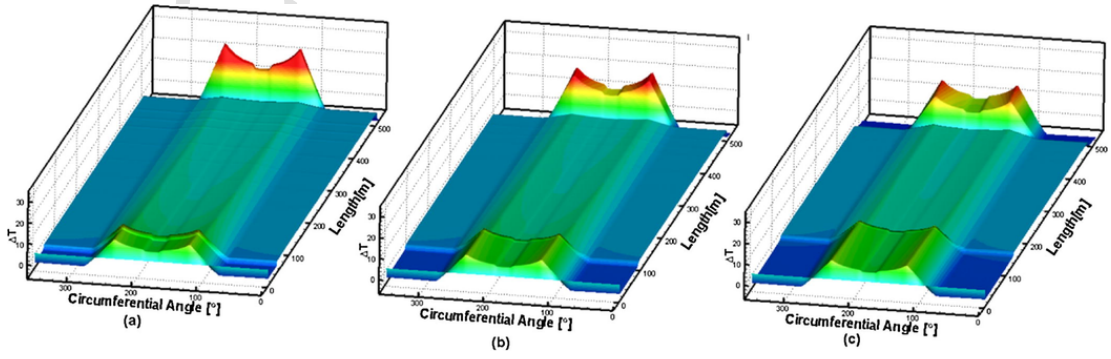

Fig. 12. Variation of the temperature difference between the absorber tube and the HTF along the DSG loop for different pressure levels. (a) 3 MPa, (b) 6 MPa and (c) 10 MPa.

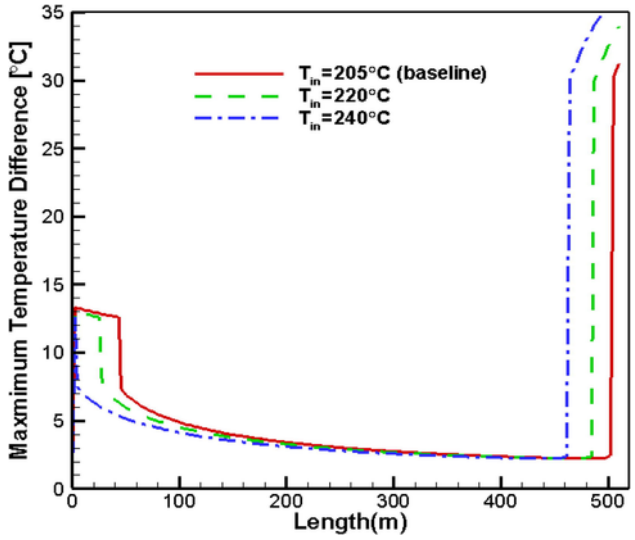

Fig. 13. Maximum temperature difference around the absorber tube for different inlet temperatures.

loop. This figure also depicts the efficiency of each section in the DSG loop.

The results show that the DSG loop is totally occupied with water flow at very low irradiance levels. After point A, the evaporation of water starts and the temperature at this section increases which makes the overall efficiency lower than the preheating efficiency. By increasing the irradiance, the efficiency of the preheating and evaporation sections keep increasing until generating superheated steam at point B. At high irradiance levels, the occupation length of the superheated section is increased which results in a decrease of the collector efficiency. This can be explained by the heat transfer coefficient distribution for different DNI levels as shown in Fig. 18. It is clear that the heat transfer coefficient is higher at the evaporation section which dominates the overall efficiency at low and medium irradiance. The dry steam has the lowest heat transfer coefficient due to the lower thermal conductivity and higher viscosity. As a consequence, the overall efficiency decreases for high radiation levels where the extent of the superheating section becomes more significant.

The DSG efficiency is also investigated with varying the mass flow rate in Fig. 19. The efficiency of the preheating and evaporation sections remains unchanged with the mass flow rate. However, the overall efficiency is affected for lower inlet water mass flow rate due to the low heat transfer coefficient of the superheating section (see Fig. 20). The effect of the superheating section is reduced when the mass flow rate is increased, which reduces the extent of the dry steam zone.

Such results are of special interest to monitor and control the DSG loop. In practice, the control of the DSG loop can be either with a fixed flow rate (similar to Fig. 17) or variable flow rate (similar to Fig. 19). The stability of the two-phase flow is also affected with the combination of the operating conditions. As discussed in Section 4.3, the pressure drop is more important at the superheating section where the speed of the steam is accelerated. Under solar radiation transients or clouds, the extent of the superheating section is reduced as shown in Fig. 18. Therefore, a significant reduction of the overall pressure drop and an increase of the mass flow rate are likely to occur leading to unstable conditions at the row outlet. According to Figs. 19 and 20, a possible solution to avoid these flow instabilities is to reduce the mass flow rate and introduce an additional pressure drop as the superheating section will recover. Therefore, control valves need to be installed at the inlet of each row to overcome the flow instabilities during clouds.

6. Conclusions

A comprehensive optical and thermo-hydraulic model is developed to predict the performance of the direct steam generation in parabolic trough solar collectors considering the non-uniform solar flux distribution around the absorber tube. Optical errors due to eccentricity and thermal bending are considered in the optical modeling to accurately determine the non-uniform solar flux distribution in the solar receiver. Results of the temperature gradient show a similar trend to the solar flux with highest thermal gradient in the concentrated region which indicate the thermal stress level. The numerical model is validated with experimental data from the DISS solar test facility for both superheat steam section and two-phase flow conditions. It is shown that the present modeling approach gives accurate results with a low computational time which indicates that the model is very reliable for the evaluation and assessment of DSG plants.

Moreover, the capability of the present methodology for analyzing the effect of different parameters on the thermal gradient around the absorber tube and the performance of the DSG loop is also presented. The flow pattern and occupancy of the three DSG sections were analyzed for different cases. It is concluded that the superheating section has the highest risk of deflection and thermal stress. An increment of the inlet pressure is favorable to increase the occupation of the preheating section and decrease the evaporation section. Although a higher pressure imposes higher pumping power, the thermal stress around the absorber tube is reduced in the superheating section. Another conclusion that can be drawn is that the increase in the inlet temperature will be accompanied with a shrinkage of the preheating section and enhancement of the annular flow in the evaporation section, while the thermal gradient is increased in the superheating section. On the other hand, solar irradiance and incident angle have comparable effects on the DSG performance. At low irradiance, the evaporation section is significantly increased and risk of stratified flow is expected. Thermal stress on the absorber tube is more pronounced for higher irradiance which is also valid for lower incident angle.

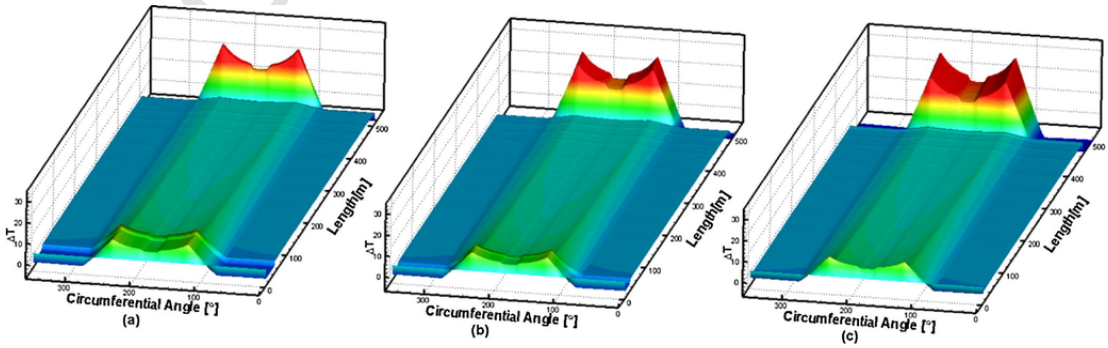

Fig. 14. Variation of the temperature difference between the absorber tube and the HTF along the DSG loop for different inlet temperature: (a) 205 °C, (b) 220 °C and (c) 240 °C.

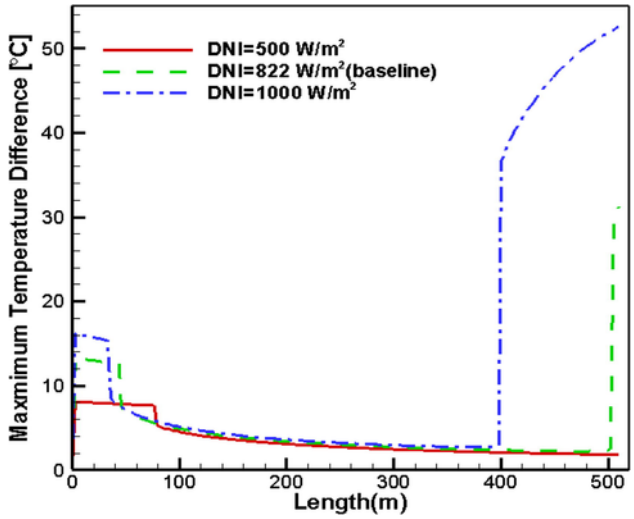

Fig. 15. Maximum temperature difference around the absorber tube for different direct normal irradiances.

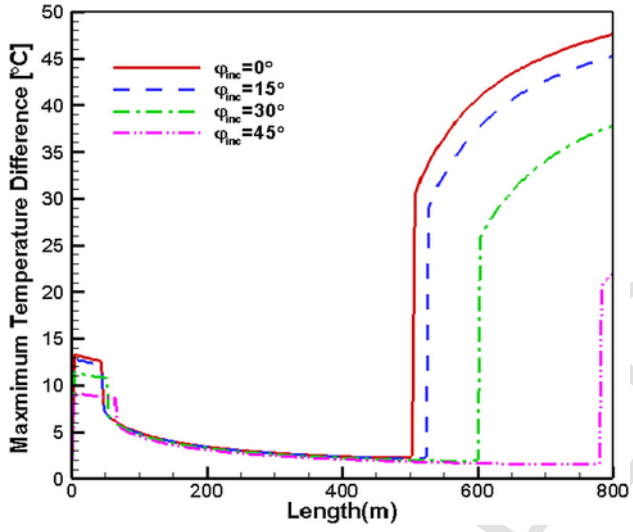

Fig. 16. Maximum temperature difference around the absorber tube for different incident angles.

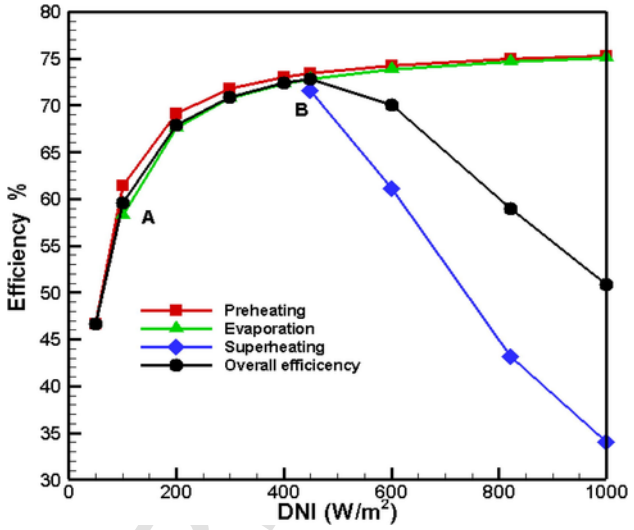

Fig. 17. Efficiency of different DSG sections and overall efficiency for various irradiance levels.

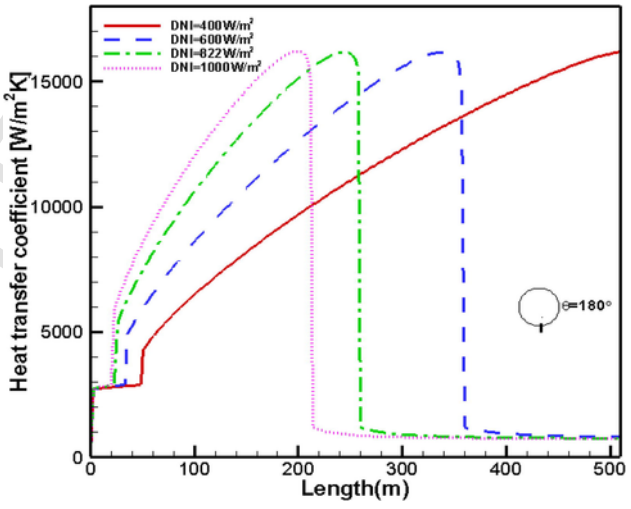

Fig. 18. Variation of the bottom heat transfer coefficient along the DSG loop for different irradiance levels.

By means of this sensitivity analysis conducted on the main parameters of the solar field loop, the present model represents a computationally efficient alternative to predict the thermo-hydraulic behavior of the parabolic trough solar collector field for direct steam generation in CSP plants working under different scenarios. Additionally, it has been shown that the model is a valuable tool for the assessment and performance evaluation of DSG loop which can be used to control and optimize such solar plants under real operating conditions. Therefore, the proposed model might be beneficial from a design point of view, as well as, for the decision making when operating this kind of plants with a direct impact on system performance and operational efficiency.

Acknowledgments

The first author is grateful for the financial support and facilities provided by the University of Sharjah under the grant V.C/G.R.C/S.R 83/2015.

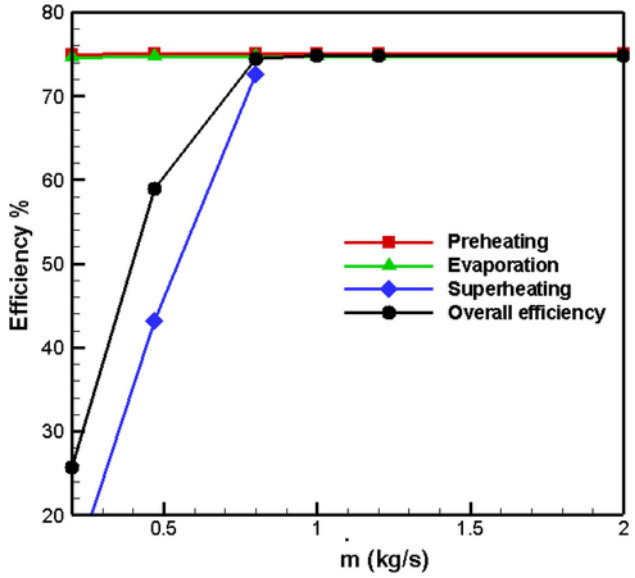

Fig. 19. Efficiency of different DSG sections and overall efficiency for various flow rates.

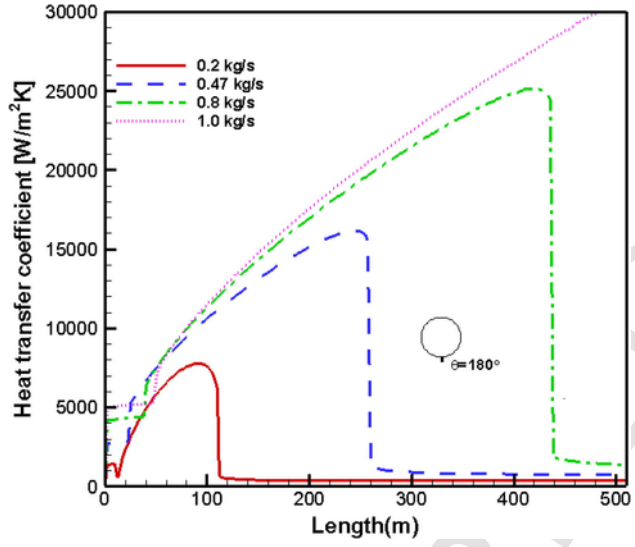

Fig. 20. Variation of the bottom heat transfer coefficient along the DSG loop for different flow rates.

References

[1] A. Fernández-García, E. Zarza, L. Valenzuela, M. Pérez, Parabolic-trough solar collectors and their applications, Renew Sustain Energy Rev 14 (7) (2010) 1695–1721.

[2] S. Mekhilef, R. Saidur, A. Safari, A review on solar energy use in industries, Renew Sustain Energy Rev 15 (4) (2011) 1777–1790.

[3] S. Kalogirou, The potential of solar industrial process heat applications, Appl Energy 76 (4) (2003) 337–361.

[4] M.W. Shahzad, K. Thu, Y.D. Kim, K.C. Ng, An experimental investigation on MEDAD hybrid desalination cycle, Appl Energy 148 (2015) 273–281.

[5] Feldhoff Jan Fabian, Benitez Daniel, Eck Markus, Riffelmann Klaus-Jürgen. Economic potential of solar thermal power plants with direct steam generation compared with HTF plants. J Solar Energy Eng 2010;132(4):041001.

[6] J.J. Serrano-Aguilera, L. Valenzuela, L. Parras, Thermal 3D model for Direct Solar Steam Generation under superheated conditions, Appl Energy 132 (2014) 370–382.

[7] A.M. Elsafi, On thermo-hydraulic modeling of direct steam generation, Solar Energy 120 (2015) 636–650.

[8] P. Wang, D.Y. Liu, C. Xu, Numerical study of heat transfer enhancement in the receiver tube of direct steam generation with parabolic trough by inserting metal foams, Appl Energy 102 (2013) 449–460.

[9] J. Muñoz, A. Abánades, Analysis of internal helically finned tubes for parabolic trough design by CFD tools, Appl Energy 88 (11) (2011) 4139–4149.

[10] W. Fuqiang, L. Qingzhi, H. Huaizhi, T. Jianyu, Parabolic trough receiver with corrugated tube for improving heat transfer and thermal deformation characteristics, Appl Energy 164 (2016) 411–424.

[11] Y. Demagh, I. Bordja, Y. Kabar, H. Benmoussa, A design method of an S-curved parabolic trough collector absorber with a three-dimensional heat flux density distribution, Solar Energy 122 (2015) 873–884.

[12] S. Guo, D. Liu, X. Chen, Y. Chu, C. Xu, Q. Liu, et al., Model and control scheme for recirculation mode direct steam generation parabolic trough solar power plants, Appl Energy 202 (2017) 700–714.

[13] D. Laing, C. Bahl, T. Bauer, D. Lehmann, W.D. Steinmann, Thermal energy storage for direct steam generation, Solar Energy 85 (4) (2011) 627–633.

[14] D. Laing, T. Bauer, N. Breidenbach, B. Hachmann, M. Johnson, Development of high temperature phase-change-material storages, Appl Energy 109 (2013) 497–504.

[15] R. Bayón, E. Rojas, L. Valenzuela, E. Zarza, J. León, Analysis of the experimental behaviour of a 100 kW th latent heat storage system for direct steam generation in solar thermal power plants, Appl Therm Eng 30 (17) (2010) 2643–2651.

[16] A. Giglio, A. Lanzini, P. Leone, M.M.R. García, E.Z. Moya, Direct steam generation in parabolic-trough collectors: a review about the technology and a thermo-economic analysis of a hybrid system, Renew Sustain Energy Rev 74 (2017) 453–473.

[17] J.M. Quibén, J.R. Thome, Flow pattern based two-phase frictional pressure drop model for horizontal tubes. Part I: Diabatic and adiabatic experimental study, Int J Heat Fluid Flow 28 (5) (2007) 1049–1059.

[18] R. Almanza, G. Jimenez, A. Lentz, A. Valdés, A. Soria, DSG under two-phase and stratified flow in a steel receiver of a parabolic trough collector, J Solar Energy Eng 124 (2) (2002) 140–144.

[19] D.H. Lobón, E. Baglietto, L. Valenzuela, E. Zarza, Modeling direct steam generation in solar collectors with multiphase CFD, Appl Energy 113 (2014) 1338–1348.

[20] Forristall R. Heat transfer analysis and modeling of a parabolic trough solar receiver implemented in engineering equation solver. National Renewable Energy Laboratory; 2003. p. 1–145.

[21] A.A. Hachicha, I. Rodríguez, R. Capdevila, A. Oliva, Heat transfer analysis and numerical simulation of a parabolic trough solar collector, Appl Energy 111 (2013) 581–592.

[22] R.V. Padilla, G. Demirkaya, D.Y. Goswami, E. Stefanakos, M.M. Rahman, Heat transfer analysis of parabolic trough solar receiver, Appl Energy 88 (12) (2011) 5097–5110.

[23] Z. Wu, S. Li, G. Yuan, D. Lei, Z. Wang, Three-dimensional numerical study of heat transfer characteristics of parabolic trough receiver, Appl Energy 113 (2014) 902–911.

[24] Q. Liu, M. Yang, J. Lei, H. Jin, Z. Gao, Y. Wang, Modeling and optimizing parabolic trough solar collector systems using the least squares support vector machine method, Solar Energy 86 (7) (2012) 1973–1980.

[25] H. Liang, S. You, H. Zhang, Comparison of different heat transfer models for parabolic trough solar collectors, Appl Energy 148 (2015) 105–114.

[26] Z.D. Cheng, Y.L. He, F.Q. Cui, B.C. Du, Z.J. Zheng, Y. Xu, Comparative and sensitive analysis for parabolic trough solar collectors with a detailed Monte Carlo ray-tracing optical model, Appl Energy 115 (2014) 559–572.

[27] S.D. Odeh, G.L. Morrison, M. Behnia, Modelling of parabolic trough direct steam generation solar collectors, Solar Energy 62 (6) (1998) 395–406.

[28] K.E. Gungor, R.H.S. Winterton, A general correlation for flow boiling in tubes and annuli, Int J Heat Mass Transfer 29 (3) (1986) 351–358.

[29] S.D. Odeh, M. Behnia, G.L. Morrison, Hydrodynamic analysis of direct steam generation solar collectors, Trans-Am. Soc. Mech. Eng. J. Solar Energy Eng. 122 (1) (2000) 14–22.

[30] Taitel Y. Flow pattern transition in two-phase flow. In: Proceeding of the 9th international heat transfer conference; 1990. p. 237–53.

[31] Eck M, Steinmann WD. Modeling and design of direct solar steam generating collector fields. In: ASME 2004 international solar energy conference. American Society of Mechanical Engineers; 2004. p. 615–24.

[32] Friedel L. Improved friction pressure drop correlations for horizontal and vertical two-phase pipe flow. In: European two-phase flow group meeting, Paper E, vol. 2; 1979. p. 1979.

[33] M.I. Roldán, L. Valenzuela, E. Zarza, Thermal analysis of solar receiver pipes with superheated steam, Appl Energy 103 (2013) 73–84.

[34] D.H. Lobón, L. Valenzuela, E. Baglietto, Modeling the dynamics of the multiphase fluid in the parabolic-trough solar steam generating systems, Energy Convers Manage 78 (2014) 393–404.

[35] Yebra LJ, Berenguel M, Zarza E, Dormido S. Object oriented modelling of DISS solar thermal power plant. In: Modelica conference, Vienna, Austria, September, 4–5; 2006.

[36] J. Bonilla, L.J. Yebra, S. Dormido, Chattering in dynamic mathematical two-phase flow models, Appl Math Model 36 (5) (2012) 2067–2081.

[37] Moya SL, Valenzuela L, Zarza E. Numerical study of the thermal-hydraulic behavior of water-steam flow in the absorber tube of the DISS system using RELAP. In: Proceedings of the international symposium solar PACES; 2011.

[38] A. Hoffmann, B. Merk, T. Hirsch, R. Pitz-Paal, Simulation of thermal fluid dynamics in parabolic trough receiver tubes with direct steam generation using the computer code ATHLET, Kerntechnik 79 (3) (2014) 175–186.

[39] M. Biencinto, L. González, L. Valenzuela, A quasi-dynamic simulation model for direct steam generation in parabolic troughs using TRNSYS, Appl Energy 161 (2016) 133–142.

[40] L. Wojtan, T. Ursenbacher, J.R. Thome, Investigation of flow boiling in horizontal tubes: Part I – a new diabatic two-phase flow pattern map, Int J Heat Mass Transfer 48 (14) (2005) 2955–2969.

[41] L. Li, J. Sun, Y. Li, Thermal load and bending analysis of heat collection element of direct-steam-generation parabolic-trough solar power plant, Appl Therm Eng (2017) https://doi.org/10.1016/j.applthermaleng.2017.08.129.

[42] Hachicha AA. Numerical simulation of a parabolic trough solar collector for hot water and steam generation. In: AIP conference proceedings, vol. 1734(1). AIP Publishing; 2016. p. 070013.
[43] A.A. Hachicha, Thermo-hydraulic modelling for Direct Steam Generation, Energy Proc 143 (2017) 705–712.
[44] R. Cundapí, S.L. Moya, L. Valenzuela, Approaches to modelling a solar field for direct generation of industrial steam, Renew Energy 103 (2017) 666–681.
[45] Y. Wang, Q. Liu, J. Lei, H. Jin, Performance analysis of a parabolic trough solar collector with non-uniform solar flux conditions, Int J Heat Mass Transfer 82 (2015) 236–249.
[46] Incropera F, DeWitt D. Fundamentals of heat and mass transfer, 3rd ed.; 1990.
[47] L. Valenzuela, E. Zarza, M. Berenguel, E.F. Camacho, Control concepts for direct steam generation in parabolic troughs, Solar Energy 78 (2) (2005) 301–311.
[48] V. Gnielinski, New equations for heat and mass transfer in turbulent pipe and channel flow, Int Chem Eng 16 (2) (1976) 359–363.
[49] L.F. Moody, Friction factors for pipe flow, Trans ASME 66 (8) (1944) 671–684.
[50] W. Wagner, A. Kruse, Properties of water and steam IAPWSIF97, Springer-Verlag, Berlin, 1998.
[51] M. Eck, E. Zarza, M. Eickhoff, J. Rheinländer, L. Valenzuela, Applied research concerning the direct steam generation in parabolic troughs, Solar Energy 74 (4) (2003) 341–351.